1-4-2010

Curvature-driven Molecular Demixing in the Budding and Breakup of Mixed Component Worm-like Miscelles

Loverde M. Sharon
University of Pennsylvania, sloverde@gmail.com

Vanessa Ortiz
University of Wisconsin - Madison

Randall D. Kamien
University of Pennsylvania

Michael L. Klein
University of Pennsylvania, Temple University

Dennis E. Discher
University of Pennsylvania, discher@seas.upenn.edu

Curvature-driven Molecular Demixing in the Budding and Breakup of Mixed Component Worm-like Miscelles

Abstract

Amphiphilic block copolymers of suitable proportions can self-assemble into surprisingly long and stable worm-like micelles, but the intrinsic polydispersity of polymers as well as polymer blending efforts and the increasing use of degradable chains all raise basic questions of curvature–composition coupling and morphological stability of these high curvature assemblies. Molecular simulations here of polyethylene glycol (PEG) based systems show that a systematic increase in the hydrated PEG fraction, in both monodisperse and binary blends, induces budding and breakup into spherical and novel 'dumbbell' micelles—as seen in electron microscopy images of degradable worm-like micelles. Core dimension, d, in our large-scale, long-time dissipative particle dynamics (DPD) simulations is shown to scale with chain-length, N, as predicted theoretically by the strong segregation limit ($d \approx N^{2/3}$), but morphological transitions of binary mixtures are only crudely predicted by simple mixture rules. Here we show that for weakly demixing diblock copolymers, the coupling between local interfacial concentration and mean curvature can be described with a simple linear relationship. The computational methods developed here for PEG-based assemblies should be useful for many high curvature nanosystems.

Disciplines

Biochemical and Biomolecular Engineering | Chemical Engineering | Engineering
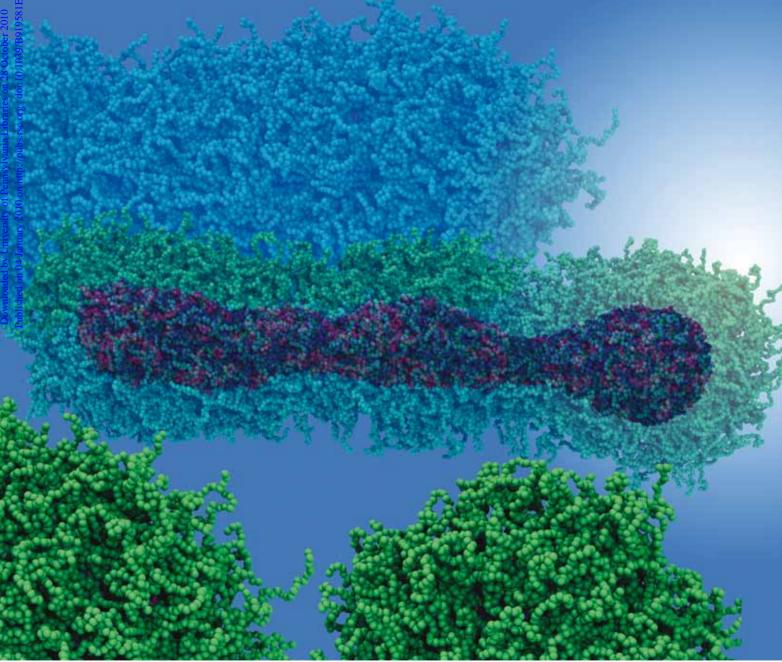
Soft Matter

RSC Publishing

PAPER
Sharon M. Loverde *et al.*
Curvature-driven molecular demixing
in the budding and breakup of mixed
component worm-like micelles

REVIEW
Michael J. Solomon and
Patrick T. Spicer
Microstructural regimes of colloidal
rod suspensions, gels, and glasses

Curvature-driven molecular demixing in the budding and breakup of mixed component worm-like micelles†

Sharon M. Loverde,*[abdf] Vanessa Ortiz,[c] Randall D. Kamien,[de] Michael L. Klein[af] and Dennis E. Discher*[be]

Amphiphilic block copolymers of suitable proportions can self-assemble into surprisingly long and stable worm-like micelles, but the intrinsic polydispersity of polymers as well as polymer blending efforts and the increasing use of degradable chains all raise basic questions of curvature–composition coupling and morphological stability of these high curvature assemblies. Molecular simulations here of polyethylene glycol (PEG) based systems show that a systematic increase in the hydrated PEG fraction, in both monodisperse and binary blends, induces budding and breakup into spherical and novel 'dumbbell' micelles—as seen in electron microscopy images of degradable worm-like micelles. Core dimension, d, in our large-scale, long-time dissipative particle dynamics (DPD) simulations is shown to scale with chain-length, N, as predicted theoretically by the strong segregation limit ($d \approx N^{2/3}$), but morphological transitions of binary mixtures are only crudely predicted by simple mixture rules. Here we show that for weakly demixing diblock copolymers, the coupling between local interfacial concentration and mean curvature can be described with a simple linear relationship. The computational methods developed here for PEG-based assemblies should be useful for many high curvature nanosystems.

Introduction

The worm-like micelle is a classic 'one-dimensional' self-assembly, but compared to vesicles or spherical micelles that can also assemble from amphiphiles worm-like micelles are less stable to perturbations. While assembly of amphiphiles in water invariably minimizes solvent-phobic contacts in the core of the micelle and maximizes solvent-philic contacts within the corona, the vesicle/worm/sphere morphologies are typically understood at a first level in terms of a packing parameter $p = v/al_c$ that is determined by molecular volume v of the packed hydrophobic segment, contour length l_c of the hydrophobic segment ($l_c \geq d/2$), and interfacial area a of the hydrophilic segment.[1] The range of p allowable for a given morphology is then calculated from core volume and interfacial area [e.g. sphere: $p = ((\pi/6)d^3)(\pi d^2 l_c)^{-1} = 0 - \frac{1}{3}$], and the cylinder-shaped worm-like micelle proves by such determinations to have a 2–3 fold narrower range of

($p = \frac{1}{3} - \frac{1}{2}$) compared to either spherical micelles or vesicle bilayers ($p = \frac{1}{2} - 1$). Despite the implied susceptibility to transitions of worm-like micelles, their unique elongated shape is increasingly being exploited in application. Worms made from low molecular weight surfactants have served as templates for inorganic frameworks[2] and as additives in oil recovery fluids.[3] Polymer-based worm micelles have taken advantage of the increased stability that arises from increasing the hydrophobic contacts with novel applications in nano-electronics and drug delivery.[4–8] Morphological transitions sometimes facilitate application and generally motivate deeper insight.

Polydispersity is unavoidable with synthetic polymers, and while degradable polymers provide one means to control morphological transitions, degradation reactions generally add complexity, as well as polydispersity. Micelles and vesicles[8] have been made from the hydrophobic and hydrolyzable polyesters poly(caprolactone) (PCL)‡ and poly(lactic acid) (PLA) as well as redox-sensitive chains such as poly(propylene sulfide) (PPS)[9] in tandem with hydrophilic polyethylene glycol (PEG) (equivalent to polyethylene oxide (PEO)). Worm-like micelles of such block copolymers appear surprisingly useful in their ability to reptate through the blood stream and permeate tumor tissues to target anticancer drugs.[10] Fragmentation into spherical micelles seems to be part of the mechanism with the hydrophobic chains

[a]Department of Chemistry, University of Pennsylvania, 231 S. 34th Street #218, Philadelphia, PA, 19104, USA. E-mail: sloverde@seas.upenn.edu; Tel: +1 215 573 0990
[b]Department of Chemical and Biomolecular Engineering, University of Pennsylvania, Philadelphia, PA, 19104, USA. E-mail: discher@seas.upenn.edu
[c]Department of Chemical and Biological Engineering, University of Wisconsin, Madison, 2014 Engineering Hall, 1415 Engineering Drive, Madison, WI, 53706-1691, USA
[d]Department of Physics and Astronomy, University of Pennsylvania, Philadelphia, PA, USA 19104
[e]Laboratory for Research on the Structure of Matter, University of Pennsylvania, Philadelphia, PA, 19104, USA
[f]Department of Chemistry, Temple University, Philadelphia, PA, 19122, USA
† Electronic supplementary information (ESI) available: Fig. SA–E and accompanying text. See DOI: 10.1039/b919581e

‡ For a degradable polymer like PCL, the degradation product after hydrolysis, 6-hydroxycaproicacid (6-HPA), is water soluble and diffuses away over experimental timescales. From separate atomistic simulations, we estimate $\chi_{PEO-PCL} = 0.146$, which corresponds to a relative interfacial tension between PEO and PCL of 2.7 mN m^{-1}, assuming a strongly segregated interface. This is a factor of ten smaller than the 30 mN m^{-1} interfacial tension measured experimentally for PEO–PEE bilayers,[39] which implies a comparably larger interfacial width w.

degrading into heterogeneous mixtures, raising fundamental questions about copolymer dispersity and micellar stability.

Here we refine and extend mesoscopic dissipative particle dynamics[11,12] (DPD) methods that are suited to long timescales (up to ms) and long polymer chains (>kDa), and we show that the DPD techniques provide an accurate means to assess both structures and transitions of polymer-based assemblies. DPD is already known to accurately capture the properties of short chain self-assemblies[13,14] and polymer solutions.[14] However, DPD can also exploit parameterizations from coarse-grained molecular dynamics (CG-MD) of diblock copolymers that not only fit all-atom models but also accurately predict structures and properties of these versatile soft materials.[15–18] Simulations here reveal the dynamic breakup of a worm-like micelle as the packing parameter is effectively decreased in both homogeneous and heterogeneous assemblies. In the latter, we test a common assumption of component additivity and then elaborate the coupling of curvature to component concentration. While such processes have been explored to some extent for a few assemblies of lipids[19–22] or peptides,[23] polymers and worm-like micelles display complex phase behavior with component poly-dispersity.[24] The simulations here probe general issues underlying the non-ergodic behavior of polymer nano-assemblies: diffusional timescales for lateral segregation within an assembly, and the coupled interplay of composition and curvature in micellar assemblies.

Computational methods

The simulation code LAMMPS[25] (large-scale atomic/molecular massively parallel simulator) was used for all simulations. The long time and length scales, as well as the correct hydrodynamics, are essential for accurate simulation of polymer morphologies relevant to applications such as drug solubilization and delivery. The DPD models for hydrophilic PEO and hydrophobic poly(ethylethylene) (PEE) used here were previously developed using a density mapping approach.[16,17] DPD refers to the use of a momentum-conserving Langevin thermostat, in combination with a soft, repulsive force interacting between the component beads and monomers. The force acting on each component bead i, f_i, consists of three contributions (conservative, dissipative, and random forces) due to neighboring beads j within a cutoff radius $r < r_c$.

$$f_i = \sum_j F_{ij}^C + F_{ij}^D + F_{ij}^R$$
$$F_{ij}^C = a_{ij}(1 - r_{ij})\hat{r}_{ij}$$
$$F_{ij}^D = -\gamma\omega_D(r_{ij})(\hat{r}_{ij}v_{ij})\hat{r}_{ij} \quad (1)$$
$$F_{ij}^R = \sigma\omega_R(r_{ij})\xi_{ij}\hat{r}_{ij}$$

where $\omega_D(r_{ij}) = \omega_R(r_{ij})^2 = (1 - r_{ij})^2$ and ξ_{ij} is a random variable with zero mean and unit variance.

The magnitudes of the random (σ) and dissipative (γ) forces are chosen such that the fluctuation–dissipation relation is obeyed ($\sigma^2 = 2k_BT\gamma$). The mass, length scales (r_c), and timescales, in addition to the self-repulsion parameters a_{ii}, are set by choosing a mapping of 3 water molecules per DPD bead. This reproduces the compressibility and diffusion of water.[11] It follows that the simulation length-scale is related to real space,

such that $r_c = 6.46$ Å, and the relation between simulation (τ) and real time is such that $\tau = 87.98$ ps.[11] All simulations here were performed with a time step δt of 0.02τ.

Average system sizes are on the order of 1300–1800 polymers with up to 2 million water beads, with timescales ranging from several μs up to 40 μs.§ Single polymers (∼40 to 140 monomers per polymer chain) can quickly aggregate, but equilibration of the micellar size distribution is not computationally accessible due to the large entropic repulsion of the chains between micellar structures.[26] True equilibrium in long chain polymeric systems is a subtle question.[26,27] Large micellar aggregates were pre-assembled and the stability of structures was assessed using DPD, to compare with experimental conditions. The micellar aggregates were prepared by 'growing' the chains from the interfacial bead inwards and outwards respectively on a cylindrical radius. Approximate core density is known (0.82 g cm^{-3}), so that this radius could be estimated accordingly after scaling with chain-length was determined. Equilibration was determined by relaxation of the micellar core density, as well as the end-to-end distance and radius of gyration of the polymer chains.

Results

Cryo-TEM images in Fig. 1a suggest that the breakup of worm micelles resembles the Rayleigh instability of a fluid stream in which interfacial perturbations propagate. The worm-like micelles of PEO–PCL ($M_n = 11\,500$ kg mol^{-1}) are initially many microns long but hydrolysis of the PCL chains promotes a progressive transition to spherical micelles and 'dumbbells'.[28] Degradation of ∼30% of the PCL has been estimated as a bulk average degradation that is necessary for budding and breakup of worms, but the reaction is heterogeneous and imaging experiments simply lack the resolution to address whether short chains localize to regions of high curvature,[28] thus motivating the DPD studies here. Simulation snapshots in Fig. 1b–f demonstrate that a mixture of copolymers with differing hydrophobic lengths undergoes a transition similar to those seen in experiments. Water molecules that surround the assembly are not shown, but the hydrated PEO corona is loose and brushy as shown in Fig. 1b with red or yellow indicating hydrophobic chains of different length. In cryo-TEM experiments, the corona is largely invisible because the PEO is also highly hydrated. Simulation snapshots in Fig. 1c–f show just the dense micelle core (as in cryo-TEM) with blue and gold now indicating the hydrophobic chains of different lengths. The two different sized chains 'appear' dispersed throughout the core, as opposed to being strictly localized to a particular curvature. Nonetheless, at some critical concentration elaborated below, segregation can be documented and undulations grow with time in the core of the worm and a sphere (or dumbbell) eventually pinches off from the worm's end-cap as shown.

The worm-to-sphere transition is a classic order-to-order transition in block copolymer melts.[29] It is also known that such transitions, if driven by a change of relative miscibility or

§ A summary of system sizes is found in Table S1†. Please note that the largest system sizes: approximately 1800 polymers and 2 000 000 waters were used for scaling results. Smaller system sizes were used to study kinetic behavior.
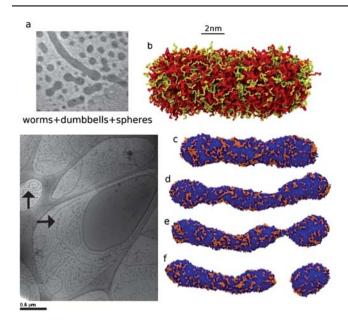
Fig. 1 Mechanism of worm-to-sphere transition. (a) Cryo-TEM images show the breakup of worm-like micelles of PEO–PCL (M_n = 11 500 kg mol^{-1}), with undulation and budding.[28] Arrows in the bottom image highlight breakup events. (b)–(f) Simulation results for a binary copolymer micelle, which details the transition dynamics. The random starting configuration of the corona (b) or core (c) with red and yellow or blue and gold respectively indicates polymers with two different length hydrophobic chains. Undulations (d) develop with bud formation (e) and pinch-off of a spherical micelle (f).

temperature can proceed *via* a metastable state that is impeded by high energy barriers and slow molecular diffusion.[30] However, large-scale mesoscopic simulations based on both detailed atomistic models, and experimental observables—as here in dilute polymer solution—can add insight into many molecular aspects of the metastable state.
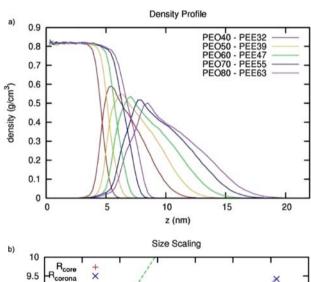
To validate the simulation physics, we step back and carefully assess the molecular weight scaling of worm-like micelle structure. In general, diblock copolymers are characterized by the total number of monomers, N_{total}, and the hydrophilic mass fraction f_{EO} ($0 \leq f_{EO} \leq 1$). The number of EO monomers, N_{EO}, plus the number of hydrophobic monomers, N_h, gives $N_{total} = N_{EO} + N_h$, and one can calculate $f_{EO} = N_{EO}m_{EO}/(N_{EO}m_{EO} + N_h m_h)$, where the m_i's are monomer masses that establish the total molecular weight of the polymer M_{tot}. Degradation of hydrophobic blocks, such as PCL, with time leads to a decrease in N_h and a net increase in f_{EO}. Phase diagrams for vesicles/worms/spheres in the (f_{EO}, M_{tot}) plane have been determined in extensive experiments on the strongly segregating block copolymers[3] simulated here, and, based on the experimental phase boundaries, an empirical correlation with the molecular packing parameter p incorporates a weak dependence on M_{tot} that can be written in a two-variable Pade' approximant form (*i.e.* as a Chisholm approximant):

$$f_{EO} \approx (0.2 - 0.01M_{tot})/(-0.03 + p - 0.01\,M_{tot}) \qquad (2)$$

This correlation for M_{tot} up to ~10 kg mol^{-1} is specifically obtained from the following correspondences: (i) p = 0.5

corresponds to where pure vesicles transition to vesicle–worm coexistence, (ii) p = 0.33 corresponds to where pure spheres transition to sphere–worm coexist, and (iii) $p = \frac{1}{2}$ (0.5 + 0.33) corresponds to the middle of the pure worm-like micelle phase. For $M_{tot} \approx 10$ kg mol^{-1} (of relevance to Fig. 1a), worm-like micelles are detected experimentally for $f_{EO} \approx 0.25$ to 0.50, with spheres—but not worms—seen in experiments for $f_{EO} > 0.50$. In the simulations below, which are among the largest and longest for atomistics-rooted DPD of polymers, we show that worm-like micelles can be kinetically stable for relatively long times (>microseconds) well above this phase boundary for both single component and binary systems.

Scaling and stability of single component worm-like micelles

First, the structural effects of increasing N_{total} at constant $f_{EO} = 0.5$ were studied with monodisperse diblock copolymer. Both experiment and theory provide scaling results for comparison. From simulations, density profiles of hydrophilic and hydrophobic monomers in the worm-like morphology depend on distance from the central axis of the micelle (Fig. 2a). As the
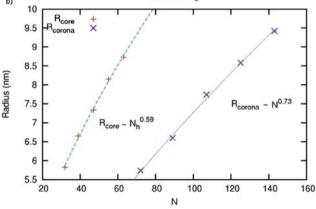

Fig. 2 Effects of diblock molecular weight on worm-like micelle structure. (a) Density profile of PEO and PEE in the worm-like morphology relative to the center of mass of the worm core. With increasing hydrophilic length of polymer at constant f_{EO}, the corona swells and polymer density in the corona decreases. (b) Scaling of radial core size, R_{core}, with the length of hydrophobic beads, N_h, and width of the corona, R_{corona}, with the total length of the polymer, $N = N_{total}$. Scaling of the core agrees well with experimental results ($R_{core} \approx N_h^{0.59}$).[29]

length of the diblock increases, the corona swells with water. Correspondingly, the polymer corona density decreases, the interfacial width between PEO and the hydrophobic block increases, and the radius of the micellar hydrophobic core scales as $\sim N_h^{0.59\,(\pm0.02)}$ (Fig. 2b). Experimental measurements of hydrophobic core diameter d by cryo-TEM show a very similar scaling of $d \approx N_h^{0.61}$.[31] The radial width of the corona, R_{corona}, scales differently with the total length of the polymer as $\sim N_{total}^{0.73}$ as shown here by simulation.

Mean-field arguments for the strong segregation limit (SSL) balance interfacial tension against chain entropy in predicting $d \approx N_h^{2/3}$; while for fully stretched chains, $d \approx N_h$. The SSL appears more similar to the simulation results. Significant end effects can also be seen for larger copolymer lengths: the end-caps become significantly more bulbous as the corona swells. This bulb formation at high molecular weights is in agreement with the experimental observation that as M_{tot} of the diblock is increased at constant f_{EO}, the preferred morphology changes from a worm to a sphere.[32]

The worm-to-sphere transition with increasing f_{EO} depends weakly on both N_{total} and the Flory–Huggins interaction parameter, χ, that specifies the relative incompatibility between blocks and that sets the cohesive energy scale for self-assembly (*i.e.* χN_{total}).[33] Simulation results for different copolymers are therefore likely to appear similar, and at least for limited studies of PEO–PCL thus far the $N_h^{2/3}$ scaling of SSL indeed also applies.[8] Additional SSL arguments[33] predict that the interfacial width varies as $w \approx (2/3\chi)^{1/2}C^{-1/2}$, where C is the concentration of polymer. In our simulations, an increase in polymer length leads to swelling of the corona and a decrease in C_{EO} with a width of the interface, w, consistent with $C_{EO}^{-0.5}$ (Fig. 2a and Fig. SE†). Consistency with SSL would also dictate a C_{EO}-dependence of interfacial tension γ,[34] $\gamma \approx (\chi/6)^{1/2}C^{3/2}$. Since γ stabilizes structure, such insights from SSL motivate the systematic analyses below the worm-to-sphere transition.
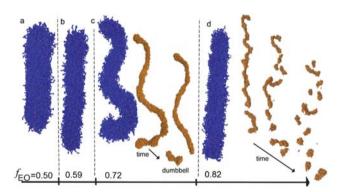

Fig. 3 Stability of single component worm-micelles with increasing f_{EO}. (a)–(d) Progressive shortening of the hydrophobic block while keeping the length of the hydrophilic block constant leads to increasing undulations in the core diameter, leading to instability and breakup at (c) f_{EO} = 0.72. The hydrophilic corona is represented in blue while the hydrophobic core is shown in gold. Instability propagates as fluctuations in the core thickness that initiate at the end of the worm, leading to bud formation at 2.4 µs and 'pinching' of a spherical micelle at 2.8 µs. Two interconnected spherical micelles give a 'dumbbell' micelle. The same process at shorter times occurs at (d) f_{EO} = 0.82, but with multiple, shorter length-scale fluctuations in the core diameter.

Stability of the worms in DPD simulation of the monodisperse copolymers was assessed by preparing individual micelles of length N_h of the hydrophobic block while holding constant the hydrophilic block length, N_{EO} (Fig. 3). An increase in temperature from ambient (293 K) to a temperature of 20% higher (352 K) showed no significant temperature effect on the meta-stability limit, consistent with experimental phase diagrams for these types of block copolymers.[30]

Increases in f_{EO} lead to an increase in fluctuations in the core (colored in gold) and a strong probability of breakup for $f_{EO} \geq 0.72$ ($\equiv f^*$). The instability typically initiates from a bulbous end of the worm, propagates as fluctuations in the core, and pinches off or buds after ~2 µs (see Table S1†). In one budding event, two interconnected or entangled spherical micelles fission from the core simultaneously. Interestingly, in the cryo-TEM images of Fig. 1a, two spherical micelles are seen to be interconnected as "dumbbells" at an experimental frequency of about 1 : 6 (dumbbell–sphere ratio). After the initial pinch-off in simulation, the timescale for additional fission is greater than several µs and only one of five simulated worm-like micelles appeared stable for ~40 µs.

For higher f_{EO} = 0.82, which should strongly favor spherical micelles, short length-scale fluctuations proliferate in the core, and the evolution should be less affected by chain-length limits to curvature-driven diffusion. A shorter timescale for pinch-off as above (~400 ns) indeed supports this argument. While micelle fusion/fission is promoted by fewer chain entanglements of shorter chains,[27] the process still takes $\sim$µs to generate distinct dumbbells and spheres (ratio 1 : 3). Simulations yield dumbbell–sphere ratios that appear remarkably similar to experimental ratios.

Copolymer mixtures in worm-like micelles: stability and breakup

Block copolymers made with degradable hydrophobic chains lose hydrophobic mass M_h and thereby increase f_{EO} with time.[8] Degradation reactions such as hydrolysis of PCL are heterogeneous in cleaving different polymer chains at different sites, so that copolymer polydispersity tends to increase with time. With simpler binary mixtures of two different miscible copolymers (A and B), additivity in mole fraction (Φ) is usually a first assumption,[22] with the phase behavior expected to reflect a mixing rule:

$$\langle f_{EO} \rangle = \Phi f_{EO,A} + (1 - \Phi) f_{EO,B} \qquad (3)$$

If such additivity applies to the DPD simulations here, the worm-to-sphere transitions for single component and multicomponent systems should prove similar. To test this additivity and also emulate degradation processes, sphere-preferring f_{EO} = 0.82 copolymer chains (PEO$_{40}$–PEE$_7$) were mixed into the otherwise stable worm-like micelles (of PEO$_{40}$–PEE$_{32}$ with f_{EO} = 0.5) and then morphological stability was assessed. Below 30 mol% of the sphere-forming copolymer, no perturbations were obvious up to ~20 µs. However, at 30 mol% ($\langle f_{EO} \rangle \approx 0.6$), peristaltic undulations along the worm micelle and perturbations in the end-caps were apparent even though the assemblies appeared stable (Fig. 4a). For mixtures of 40 mol% sphere-former and above ($\langle f_{EO} \rangle \geq 0.63$), perturbations in the micellar
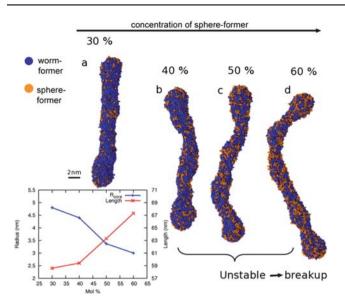
Fig. 4 Effects of mixing on worm-like micelle stability. Radial undulations that precede breakup and budding into spherical micelles, as a function of concentration of PEO_{40}–PEE_7 ($f_{EO} = 0.82$) in a PEO_{40}–PEE_{32} worm. The hydrophobic blocks of the sphere and worm formers are shown in orange and blue, respectively. (a) At 30 mol% PEO_{40}–PEE_7, the worm assembly remains stable for the total length of the simulation of 20 μs. (b)–(d) At 40 mol% PEO_{40}–PEE_7 or higher, increasing undulations and core thickness fluctuations, as observed here, lead to eventual breakage of the worm morphology (as shown in Fig. 1) within the time of the simulation. Also shown, average hydrophobic core radius, R_{core}, and worm contour length before breakup as a function of sphere-former concentration.

density profiles were extreme and, with time, radial undulations on a length-scale of spherical micelle dimensions precede budding and breakup into spherical micelles as shown in Fig. 1. Interestingly, individual unimers of PEO_{40}–PEE_7, but not of PEO_{40}–PEE_{32}, are expelled just prior to the first spherical micelle fission process. While this indicates that the free energy of transfer for unimers is lower for the short chain than the micelle fission energy, it also suggests that the critical $\langle f_{EO}\rangle^*$ for the transition will be somewhat over-estimated with this short, fully segregating copolymer. The fact that f^* for the single component system is similar to but different from $\langle f_{EO}\rangle^*$ motivates a deeper, analytical understanding of block copolymer mixtures—as pursued theoretically in the final section below.

Coupling of curvature to concentration

Mean-field models of the worm-to-sphere transition for charged diblock copolymers can reproduce—with some key assumptions—the phase behavior of diblock copolymer micelles as a function of charge fraction on the polymer and salt concentration in solution.[35] Such models have been based in part on a 'metastable unduloid' phase observed experimentally with poly(acrylic acid)–poly(styrene) PAA–PS,[36] but the transition in shape is assumed *ad hoc* to occur in three stages: neck contraction, scission, and finally budding with end relaxation. Scission should expose unfavorable contacts with water, and the simulations here indeed show that hydrophobic contacts are exposed at the breaking point—with the noted liberation of unimers

providing obvious evidence. Furthermore, with increasing mol% of the sphere-former, the average core size decreases before breakup and the worm elongates (Fig. 4, inset). The volume decreases by up to ~20% and the number of spherical micelles that bud off increases (from three to six). The density profile of the core of the mixed micelle shows that the short hydrophobic tails localize close to the interface and reduce the core density by a factor of ~$^7/_{10}$. In other words, the free volume for the longer hydrophobic chains increases, which is consistent with theory,[37] but insight into molecular demixing has been lacking.

The line tension between domains in vesicles composed of strongly segregating amphiphiles is one of the main driving forces for curvature and budding.[38,39] Oftentimes, concentration can even act in the reverse manner—to stabilize new phases, such as concentrated hydrogels containing lipids that act to reduce the symmetry of the multilamellar phase through dislocation defects.[40] With amphiphiles that demix weakly as simulated here (Fig. 1), the degree of local correlations between curvature and molecular concentration during the evolution of the 'metastable unduloid' structure (Fig. 4) is of utmost interest. Fig. 5 demonstrates the procedure to extract correlations between local diblock concentrations at the interface and mean curvature, H. For timescales during which undulations were significant, up until timescales immediately preceding pinching and break-off of the initial spherical micelle, we find the location of the interface for each axial worm slice—defined by the average position of the interfacial copolymer beads in each slice. The interfacial profile between the hydrophilic PEO and hydrophobic PEE along the worm axis is then fit with a polynomial of degree six. Next, we calculate the interfacial polymer concentration (N_{poly}/A) along
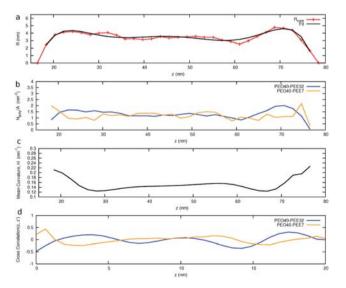

Fig. 5 Sample polynomial fit and associated calculations for correlation between concentration and mean curvature, H. From top to bottom: (a) sample interfacial axial worm profile and associated polynomial fit at $t = 789$ ns for 40 mol% as shown in Fig. 4, (b) interfacial polymer concentration, N_{poly}/A for PEO_{40}–PEE_7 and PEO_{40}–PEE_{32} along the axial worm profile at $t = 789$ ns for 40 mol%, (c) mean curvature, H, and, finally, cross-correlation between concentration and (d) mean curvature, H, as a function of the axial distance along the worm.

the worm axis for each of the diblocks. The mean curvature, H, is then calculated as:

$$H = \tfrac{1}{2} [(1/g)(1 + g'^2)^{-1/2} - (g'')(1 + g'^2)^{-3/2}] \tag{4}$$

where g is the polynomial fit to the interface and, lastly, the cross-correlation between ϕ and H is then calculated as:

$$\chi_{\phi,H}(d) = \frac{\sum_z \left[(H_z - \overline{H})(\phi_{z+d} - \overline{\phi})\right]}{\sqrt{\sum_z (H_z - \overline{H})^2} \sqrt{\sum_z (\phi_{z+d} - \overline{\phi})^2}} \tag{5}$$

A positive correlation between PEO_{40}–PEE_7 and mean curvature is shown in Fig. 5 while PEO_{40}–PEE_{32} is anti-correlated with mean curvature. Moreover, the cross-correlation function along the axis of the worm shows strong fluctuations. The shorter chains thus prefer the more bulbous regions and the end-caps, as opposed to the thinner radial regions of the worm.

We assume the local mean curvature is a linear superposition of the two mean curvatures, H_1 and H_2, from the unmixed states:

$$H(\phi) = \phi H_1 + (1 - \phi)H_2 \tag{6}$$

H_1 (1/3.87 nm^{-1}) and H_2 (1/14.4 nm^{-1}) are spherical and cylindrical mean curvatures of single component micelles as obtained by simulations as shown in Fig. 3. We plot the mean curvature, H, vs. ϕ (where ϕ is the normalized interfacial concentration of PEO_{40}–PEE_7), for a range of timescales during which undulations were significant in Fig. 6. ϕ is calculated for local axial worm slices, excluding the tips of the worm micelle,¶ assuming
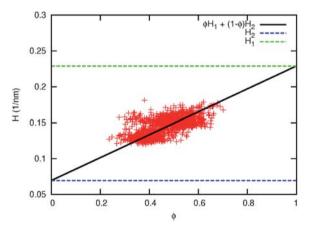

Fig. 6 Mean curvature, H, vs. ϕ (where ϕ is the normalized interfacial concentration of PEO_{40}–PEE_7) and fit, using calculated mean curvatures, H_1, spherical mean curvature, and H_2, cylindrical mean curvature from simulations of single component polymer assemblies as shown in Fig. 3. We show that a concentration averaged mean curvature is a good approximation for the local curvature. This plot is for the main body of the worm micelle, excluding the end-caps, where higher interfacial concentrations are found.

¶ It is found that there are deviations from this behavior at high concentrations of the minority component along the length of the micelle, which is the end-cap region, that does not fit this linear behavior, and may be subject to the finite size effects.

a projected cylindrical surface area. At all interfacial concentrations of PEO_{40}–PEE_7, the behavior of ϕ is clearly linear with H, and supports a spontaneous curvature that depends as a linear superposition of the two equilibrium mean curvatures, H_1 and H_2. This linear relationship between interfacial concentration, ϕ, and mean curvature holds for both mole fractions, $\Phi = 30$ mol% and 40 mol% simulations, one in which a kinetically stable worm exhibits interfacial fluctuations, the other in which the fluctuations lead to budding and breakup.

Sorting of lipids[20] or membrane proteins, such as CTB (cholera toxin subunit B), through curvature, is suggested to be dependent on their ability to sense membrane shape.[41] Theory suggests that non-linear corrections are necessary near a critical demixing point.[42] Here we show that for a simple diblock copolymer mixture in a kinetically evolving micelle, differing purely in terms of the packing parameter of the chains, the micellar shape is coupled to the local interfacial concentration in a simple linear relationship.

Conclusions

Equilibrium properties and scaling behavior of polymer-based worm-like micelles were elaborated together with analyses of the kinetic stability of both monodisperse and mixed assemblies. The scaling of an isolated worm micelle core with the length of hydrophobic tail of the copolymer at constant hydrophilic fraction, $d \approx N_h^{0.59}$, agrees well with experimental results, and is consistent with scaling within the strong segregation limit. The PEG corona swells with increased copolymer length, and an increase in hydrophilic fraction to $f_{EO} = 0.72$ destabilizes the worm-like micelle to Rayleigh-like budding from the end-caps.

In a mixture, the diffusive properties of the copolymers at the interface suggest reptation dynamics (see ESI†), and we find that the shorter copolymer localizes close to the interface and acts to reduce the overall core density. Flexibility of the worm micelle before breakup can be determined from careful modeling of curvature-driven segregation and seems to be consistent with experiment. A metastable mixed copolymer worm also disassembles through dynamic undulation and budding, providing novel insight into the type of breakup that has already been exploited in delivery of anticancer drugs.[10] Dissipative particle dynamics simulations accurately capture many of the complex processes and transformations across relevant time and length scales, and so DPD seems to be a useful method for molecular-scale investigations of the many PEG-based systems being developed for a wide range of applications.

Acknowledgements

Notes and references

1 J. N. Israelachvili, *Intermolecular and Surface Forces*, Academic Press, London, 1992.
2 S. A. Bagshaw, E. Prouzet and T. J. Pinnavaia, *Science*, 1995, **269**, 1242–1244.
3 K. C. Taylor and H. A. Nasr-El-Din, *J. Petrol. Sci. Eng.*, 1998, **19**, 265–280.
4 S. Jain and F. S. Bates, *Science*, 2003, **300**, 460–464.
5 S. Karaborni, E. Esselink, P. A. J. Hilbers, B. Smit, J. Karthauser, N. M. van Os and R. Zana, *Science*, 1994, **266**, 254–256.
6 X. S. Wang, G. Guerin, H. Wang, Y. Wang, I. Manners and M. A. Winnik, *Science*, 2007, **317**, 644–647.
7 H. G. Cui, Z. Y. Chen, S. Zhong, K. L. Wooley and D. J. Pochan, *Science*, 2007, **317**, 647–650.
8 Y. Geng and D. E. Discher, *Polymer*, 2006, **47**, 2519–2525.
9 A. Napoli, M. Valentini, N. Tirelli, M. Muller and J. A. Hubbell, *Nat. Mater.*, 2004, **3**, 183–189.
10 Y. Geng, P. Dalhaimer, S. Cai, R. Tsai, M. Tewari, T. Minko and D. E. Discher, *Nat. Nanotechnol.*, 2007, **2**, 249–255.
11 R. D. Groot and P. B. Warren, *J. Chem. Phys.*, 1997, **107**, 4423–4435; R. D. Groot, *Applications of Dissipative Particle Dynamics, Novel Methods in Soft Matter Simulations*, Springer-Verlag, Berlin Heidelberg, 2004.
12 C. M. Wijmans, B. Smit and R. D. Groot, *J. Chem. Phys.*, 2001, **114**, 7644–7654.
13 A. Grafmuller, J. Shillcock and R. Lipowsky, *Phys. Rev. Lett.*, 2007, **98**, 218101.
14 L. Rekvig, B. Hafskjold and B. Smit, *J. Chem. Phys.*, 2004, **120**, 4897–4905.
15 G. Srinivas, D. E. Discher and M. L. Klein, *Nat. Mater.*, 2004, **3**, 638–644.
16 V. Ortiz, S. O. Nielsen, D. E. Discher, M. L. Klein, R. Lipowsky and J. Shillcock, *J. Phys. Chem. B*, 2005, **109**, 17708–17714.
17 V. Ortiz, S. O. Nielsen, M. L. Klein and D. E. Discher, *J. Polym. Sci., Part B: Polym. Phys.*, 2006, **44**, 1907–1918.
18 G. Srinivas and J. W. Pitera, *Nano Lett.*, 2008, **8**, 611–618.
19 D. M. Cooke and A. C. Shi, *Macromolecules*, 2006, **39**, 6661–6671.
20 I. R. Cooke and M. Deserno, *Biophys. J.*, 2006, **91**, 487–495.
21 G. van Meer, *EMBO Rep.*, 2005, **6**, 418–419; V. V. Kumar, *Proc. Natl. Acad. Sci. U. S. A.*, 1991, **88**, 444–448.
22 V. V. Kumar, *Proc. Natl. Acad. Sci. U. S. A.*, 1991, **88**, 444–448.
23 B. J. Reynwar, G. Ilya, V. A. Harmandaris, M. M. Mueller, K. Kremer and M. Derserno, *Nature*, 2007, **447**, 461–464.
24 K. P. Davis, T. P. Lodge and F. S. Bates, *Macromolecules*, 2008, **41**, 8289–8291.
25 S. Plimpton, *J. Comput. Phys.*, 1995, **117**, 1–19.
26 A. N. Semenov, *Zh. Eksp. Teor. Fiz.*, 1985, **88**, 1242–1256.
27 E. E. Dormidontova, *Macromolecules*, 1999, **32**, 7630–7644.
28 Y. Geng and D. E. Discher, *J. Am. Chem. Soc.*, 2005, **127**, 12780–12781.
29 C. Y. Ryu and T. P. Lodge, *Macromolecules*, 1999, **32**, 7190–7201.
30 D. A. Hajduck, H. Takenouchi, M. A. Hillmyer, F. S. Bates, M. E. Vigild and K. Almdal, *Macromolecules*, 1997, **30**, 3788–3795.
31 P. Dalhaimer, F. S. Bates and D. E. Discher, *Macromolecules*, 2003, **36**, 6873–6877.
32 P. Dalhaimer, H. Bermudez and D. E. Discher, *J. Polym. Phys., Part B*, 2004, **4**, 168–176.
33 M. J. Schick, *Nonionic Surfactants: Physical Chemistry*, Marcel Dekker, Inc., NY, 1987.
34 J. Noolandi and K. M. Hong, *Macromolecules*, 1983, **16**, 1443–1448.
35 D. Bendejacq, M. Joanicot and V. Ponsinet, *Eur. Phys. J. E*, 2005, **17**, 83–92.
36 G. M. Grason and C. D. Santangelo, *Eur. Phys. J. E*, 2006, **20**, 335–346.
37 I. Szleifer, D. Kramer, A. Ben-Shaul, D. Roux and W. M. Gelbart, *Phys. Rev. Lett.*, 1988, **60**, 1966–1969.
38 B. Huttner and J. Zimmerberg, *Curr. Opin. Cell Biol.*, 2001, **13**, 478–484.
39 T. Baumgart, S. T. Hess and W. W. Webb, *Nature*, 2003, **425**, 821–824.
40 H. E. Warriner, S. H. J. Idziak, N. L. Slack, P. Davidson and C. R. Safinya, *Science*, 1996, **271**, 969–973.
41 A. Tian and T. Baumgart, *Biophys. J.*, 2009, **96**, 2676–2688.
42 U. Seifert, *Phys. Rev. Lett.*, 1993, **70**, 1335–1338.